Acta Mech 230, 1999–2012 (2019)
https://doi.org/10.1007/s00707-019-2364-y

ORIGINAL PAPER

V. Govorukha · A. Sheveleva · M. Kamlah

A crack along a part of an interface electrode in a piezoelectric bimaterial under anti-plane mechanical and in-plane electric loadings

Received: 23 September 2018 / Revised: 17 December 2018 / Published online: 16 February 2019

Abstract An electrically conducting crack along a part of an electrode in the interface of a piezoelectric bimaterial under the action of anti-plane mechanical and in-plane electric loadings is analyzed. The electrode is assumed to be much thinner than the piezoelectric material, and therefore, its mechanical properties are neglected. Using special representations of field variables via sectionally analytic functions, a combined Dirichlet–Riemann boundary value problem is formulated and solved analytically. Explicit expressions for the shear stress, the electric field and the crack faces' sliding displacement are derived. These quantities are also presented graphically along the corresponding parts of the material interface. The intensity factors for stress and electric field are determined as well. The dependencies of the mentioned values on the magnitude of the external electric loading and different ratios of the crack and electrode lengths are presented.

1 Introduction

Due to their high electromechanical coupling effect, piezoelectric materials are widely used in many fields of modern engineering. Usually, these materials are integrated into complex smart composite structures, which have become attractive candidates for use in sensors, transducers and actuators. These composite structures are operated under high electric and mechanical loads. The electric loads are often applied to devices by means of some compliant foil-shaped metal electrodes embedded into interfaces. However, because of the brittleness and the low strength of piezoelectric materials, a high electric field may give rise to debonding and delamination between the embedded thin electrode and the piezoelectric matrix. Such a phenomenon has been observed in experiments [2,3]. Therefore, it is very important to study the behavior of piezoelectric composites with interface defects subjected to the action of mechanical stresses and electrical fields.

Piezoelectric devices with internal electrodes embedded at a bimaterial interface have been actively studied in recent years [1,12,13,24,26]. One of the central topics was focused on the boundary conditions at the electrodes. Three different kinds of electrode models have been put forward for the electroelastic analysis of piezoelectric structures, including the rigid line inclusion model [1], the mechanically compliant model [24], and the crack-type model [11]. In practice, electrodes generally can be considered as metal foils, which are more flexible than the surrounding piezoelectric materials. For this reason, the mechanically compliant model has been widely employed by researchers. Besides, theoretical analysis and numerical results have also shown that the edge of the electrode is a potential position of high stress and electric field concentrations [14,18].

V. Govorukha (✉) · A. Sheveleva
Department of Computational Mathematics, Oles Honchar Dnipro National University, Gagarin Av. 72, Dnipro 49010, Ukraine
E-mail: govorukhavb@yahoo.com

M. Kamlah
Institute of Applied Materials, Karlsruhe Institute of Technology, Hermann-von-Helmholtz-Platz 1,
76344 Eggenstein-Leopoldshafen, Germany
E-mail: marc.kamlah@kit.edu

It should be noted that the above-cited works are devoted to the electrodes without cracks. In fact, experiments have demonstrated [29] that cracks are formed preferentially at the interface between the electrode and the piezoelectric matrix. For such cracks, considerable research work on the analysis of electric and elastic behaviors has been made. For example, Ru [25] derived the exact solutions for a single interface crack situated on one side of the electrode layer and for a pair of interface cracks situated symmetrically on the opposite sides of the electrode layer. Häusler et al. [8] and Häusler and Balke [7] studied the generalized two-dimensional problems of collinear and periodic electrode–ceramic interface cracks in piezoelectric bimaterials and gave the expressions of the singular fields at the tip of the electrode. A general treatment for generalized two-dimensional problems in anisotropic piezoelectric bimaterials with interface defects has been developed by Wang and Shen [28]. In some cases, a finite length electrode can completely exfoliate together with some part of the material interface, forming a partially conductive interface crack. This problem has been solved in closed form by Lapusta et al. [10]. An arc-shaped conducting rigid line inclusion located at the interface between a circular piezoelectric inhomogeneity and an unbounded piezoelectric matrix subjected to remote uniform anti-plane shear stresses and in-plane electric fields has been considered by Wang and Schiavone [27]. Recently, Onopriienko et al. [19] studied the interaction of a conductive crack and an electrode at a piezoelectric bimaterial interface. Simple analytical expressions for the stress, the electric field, and their intensity factors as well as for the crack faces displacement jump have been derived. A more detailed review of the investigation of in-plane and anti-plane crack problems in piezoelectric bimaterials can be found in the review paper by Govorukha et al. [4].

The present work is devoted to the analysis of electrode–ceramic interface cracks in piezoelectric bimaterials under the action of anti-plane mechanical and in-plane electric loadings. The piezoelectric materials located at the two sides of the finite length interface electrode are assumed to be transversely isotropic and the crack to be conducting. The crack is formed on one side of an interface electrode. It covers only some part of the electrode, and therefore, uncracked zones remain either at both or at one of the electrode edges. This leads to a nontrivial mixed boundary value problem which becomes mathematically much more complicated than the associated problem for a crack along the whole electrode. To the best of our knowledge, the analytical solutions of this problem have not been obtained yet. In this paper, such a solution is derived and some immediate consequences of the obtained solution are discussed.

2 Basic equations

In the absence of body forces and free electric charges, the basic equations for a linear piezoelectric material presented, for example, by Parton and Kudryavtsev [23] include the constitutive equations

$$\sigma_{ij} = c_{ijmn}\gamma_{mn} - e_{mij}E_m, \quad D_i = e_{imn}\gamma_{mn} + \varepsilon_{im}E_m, \tag{1}$$

the equilibrium equations

$$\sigma_{ij,j} = 0, \quad D_{i,i} = 0, \tag{2}$$

and the gradient equations

$$\gamma_{ij} = \frac{1}{2}\left(u_{i,j} + u_{j,i}\right), \quad E_i = -\varphi_{,i}, \tag{3}$$

where $i, j, m, n = 1, 2, 3$; σ_{ij}, γ_{ij}, D_i, E_i, u_i, and φ are the components of stress, strain, electric displacement, electric field, mechanical displacement, and electric potential, while c_{ijmn}, e_{ijm}, and ε_{ij} are the elastic, piezoelectric, and dielectric constants, respectively; repeated indices imply summation (from 1 to 3). The subscript comma denotes partial derivative with respect to the rectangular Cartesian coordinates $x_i (i = 1, 2, 3)$.

In this paper, we will focus our attention on transversely isotropic piezoelectric materials with hexagonal symmetry (piezoceramics), which have an isotropic basal plane parallel to the (x_1, x_2)-plane and a poling direction parallel to the x_3-axis. Materials of this symmetry class have been used for many different industrial purposes due to their high piezoelectric coupling coefficients.

Let the piezoelectric solid be subject to combined anti-plane mechanical and in-plane electric loads. In this case, only the out-of-plane displacement u_3 and the electric potential φ, which are independent of x_3, will not vanish, i.e.,

$$u_1 = u_2 = 0, \quad u_3 = u_3(x_1, x_2), \quad \varphi = \varphi(x_1, x_2),$$

and the constitutive equations (1) can be simplified as [20]

$$\sigma_{13} = c_{44}\frac{\partial u_3}{\partial x_1} + e_{15}\frac{\partial \varphi}{\partial x_1}, \quad \sigma_{23} = e_{44}\frac{\partial u_3}{\partial x_2} + e_{15}\frac{\partial \varphi}{\partial x_2},$$
$$D_1 = e_{15}\frac{\partial u_3}{\partial x_1} - \varepsilon_{11}\frac{\partial \varphi}{\partial x_1}, \quad D_2 = e_{15}\frac{\partial u_3}{\partial x_2} - \varepsilon_{11}\frac{\partial \varphi}{\partial x_2}. \tag{4}$$

The equilibrium equations (2) become

$$c_{44}\nabla^2 u_3 + e_{15}\nabla^2\varphi = 0,$$
$$e_{15}\nabla^2 u_3 - \varepsilon_{11}\nabla^2\varphi = 0, \tag{5}$$

where $\nabla^2 = \partial^2/\partial x_1^2 + \partial^2/\partial x_2^2$ is the two-dimensional Laplacian operator. Due to $e_{15}^2 + c_{44}\varepsilon_{11} \neq 0$, the above equations can be reduced to two decoupled Laplace equations

$$\nabla^2 u_3 = 0, \quad \nabla^2\varphi = 0. \tag{6}$$

Equation (6) indicates that out-of-plane displacement u_3 and electric potential φ are harmonic functions and, thus [9], they can be expressed as real parts of arbitrary analytic functions $f_1(z)$ and $f_2(z)$ of a complex variable $z = x_1 + ix_2$ in the way

$$u_3 = 2\mathrm{Re}\, f_1(z), \quad \varphi = 2\mathrm{Re}\, f_2(z), \tag{7}$$

where 'Re' denotes the real part of an analytic function and $i = \sqrt{-1}$.

Introducing further the vector-functions

$$\mathbf{u} = [u_3, \varphi]^{\mathrm{T}}, \quad \mathbf{f}(z) = [f_1(z), f_2(z)]^{\mathrm{T}},$$

the relations (7) can be written in the form

$$\mathbf{u} = \mathbf{A}\mathbf{f}(z) + \bar{\mathbf{A}}\bar{\mathbf{f}}(\bar{z}). \tag{8}$$

Substituting the representation (8) into (4), we have

$$\mathbf{t} = \mathbf{B}\mathbf{f}'(z) + \bar{\mathbf{B}}\bar{\mathbf{f}}'(\bar{z}), \tag{9}$$

where $\mathbf{t} = [\sigma_{23}, D_2]^{\mathrm{T}}$, $\mathbf{f}'(z) = \left[f_1'(z), f_2'(z)\right]^{\mathrm{T}}$. Here and afterward, the superscript 'T' denotes transposition of a matrix, the overbar stands for the complex conjugate and prime ($'$) implies the derivative with respect to the associated arguments. Here $\mathbf{A}$ and $\mathbf{B}$ are the 2×2 matrices defined by

$$\mathbf{A} = \begin{bmatrix} 1 & 0 \\ 0 & 1 \end{bmatrix}, \quad \mathbf{B} = i\begin{bmatrix} c_{44} & e_{15} \\ e_{15} & -\varepsilon_{11} \end{bmatrix}.$$

The explicit form of Eqs. (8) and (9) is not appropriate for solving the problem for electrode–ceramic interface crack considered here based on the extended Stroh formalism. Therefore, we introduce the new vector-functions

$$\mathbf{v} = \left[\frac{\partial u_3}{\partial x_1}, D_2\right]^{\mathrm{T}}, \quad \mathbf{p} = [\sigma_{23}, E_1],$$

and using the presentations (3), (8) and (9), these vector-functions can be written as

$$\mathbf{v} = \mathbf{M}\mathbf{f}'(z) + \bar{\mathbf{M}}\bar{\mathbf{f}}'(\bar{z}), \tag{10}$$
$$\mathbf{p} = \mathbf{N}\mathbf{f}'(z) + \bar{\mathbf{N}}\bar{\mathbf{f}}'(\bar{z}), \tag{11}$$

where the matrices $\mathbf{M}$ and $\mathbf{N}$ are defined by means of the reconstruction of the matrices $\mathbf{A}$ and $\mathbf{B}$ in the form

$$\mathbf{M} = \begin{bmatrix} 1 & 0 \\ ie_{15} & -i\varepsilon_{11} \end{bmatrix}, \quad \mathbf{N} = \begin{bmatrix} ic_{44} & ie_{15} \\ 0 & -1 \end{bmatrix}.$$

3 General solution of the basic equations

First, we get more general representations, from which the fracture mechanics problem of this work can be obtained as a special case. Consider a bimaterial composite, which consists of two piezoelectric half-planes $x_2 > 0$ and $x_2 < 0$ of different material properties. We assume that the stress and the tangential component of the electric field are continuous across the whole bimaterial interface. Furthermore, the mechanically and electrically bonded part of the interface is denoted by L. Then, the boundary conditions at the interface $x_2 = 0$ are

$$\sigma_{23}^{(1)}(x_1, 0) = \sigma_{23}^{(2)}(x_1, 0), \quad E_1^{(1)}(x_1, 0) = E_1^{(2)}(x_1, 0), \quad \text{for } x_1 \in (-\infty, \infty), \tag{12}$$

$$\gamma_{13}^{(1)}(x_1, 0) = \gamma_{13}^{(2)}(x_1, 0) \quad D_2^{(1)}(x_1, 0) = D_2^{(2)}(x_1, 0), \quad \text{for } x_1 \in L, \tag{13}$$

where the subscripts 1 and 2 refer to the materials in $x_2 > 0$ and $x_2 < 0$, respectively.

To solve this problem, we use the representations (10) and (11) for the upper ($k = 1$) and lower ($k = 2$) half-planes, which can be written in the form

$$\mathbf{v}^{(k)} = \mathbf{M}^{(k)}\mathbf{f}'^{(k)}(z) + \bar{\mathbf{M}}^{(k)}\bar{\mathbf{f}}'^{(k)}(\bar{z}), \tag{14}$$

$$\mathbf{p}^{(k)} = \mathbf{N}^{(k)}\mathbf{f}'^{(k)}(z) + \bar{\mathbf{N}}^{(k)}\bar{\mathbf{f}}'^{(k)}(\bar{z}). \tag{15}$$

According to the continuity conditions (12) and the relations (15), we get

$$\mathbf{N}^{(1)}\mathbf{f}'^{(1)}(x_1 + i0) + \bar{\mathbf{N}}^{(1)}\bar{\mathbf{f}}'^{(1)}(\overline{x_1 + i0}) = \mathbf{N}^{(2)}\mathbf{f}'^{(2)}(x_1 - i0) + \bar{\mathbf{N}}^{(2)}\bar{\mathbf{f}}'^{(2)}(\overline{x_1 - i0}),$$

which can be rewritten as

$$\mathbf{N}^{(1)}\mathbf{f}'^{(1)}(x_1 + i0) - \bar{\mathbf{N}}^{(2)}\bar{\mathbf{f}}'^{(2)}(x_1 + i0) = \mathbf{N}^{(2)}\mathbf{f}'^{(2)}(x_1 - i0) - \bar{\mathbf{N}}^{(1)}\bar{\mathbf{f}}'^{(1)}(x_1 - i0), \quad x_1 \in (-\infty, \infty). \tag{16}$$

The left-hand side of Eq. (16) is the boundary value of a function being analytic in the upper half-plane, and the right-hand side is the boundary value of another function being analytic in the lower half-plane. Hence, both functions are equal to a function, defined as

$$\mathbf{J}(z) = \begin{cases} \mathbf{N}^{(1)}\mathbf{f}'^{(1)}(z) - \bar{\mathbf{N}}^{(2)}\bar{\mathbf{f}}'^{(2)}(z), & x_2 > 0, \\ \mathbf{N}^{(2)}\mathbf{f}'^{(2)}(z) - \bar{\mathbf{N}}^{(1)}\bar{\mathbf{f}}'^{(1)}(z), & x_2 < 0, \end{cases} \tag{17}$$

which is analytic in the whole plane.

Assuming that the stress and electric field are bounded at infinity, it follows that $\mathbf{J}(\infty) = \mathbf{J}^{\infty}$, where $\mathbf{J}^{\infty}$ is a constant vector. But according to Liouville's theorem, this means that $\mathbf{J}(z) = \mathbf{J}^{\infty}$ holds true in the whole plane. Thus, from Eq. (17), it follows that

$$\begin{aligned} \mathbf{N}^{(1)}\mathbf{f}'^{(1)}(z) - \bar{\mathbf{N}}^{(2)}\bar{\mathbf{f}}'^{(2)}(z) &= \mathbf{J}^{\infty}, \ x_2 > 0, \\ \mathbf{N}^{(2)}\mathbf{f}'^{(2)}(z) - \bar{\mathbf{N}}^{(1)}\bar{\mathbf{f}}'^{(1)}(z) &= \mathbf{J}^{\infty}, \ x_2 < 0. \end{aligned} \tag{18}$$

Since $\mathbf{f}^{(k)}(z)(k = 1, 2)$ are arbitrary vector-functions, one can choose $\mathbf{J}^{\infty} = [0, 0]^{\mathrm{T}}$. Taking into account that the matrices in Eq. (18) are nonsingular, one obtains

$$\begin{aligned} \bar{\mathbf{f}}'^{(2)}(z) &= \left(\bar{\mathbf{N}}^{(2)}\right)^{-1}\mathbf{N}^{(1)}\mathbf{f}'^{(1)}(z), \ x_2 > 0, \\ \mathbf{f}'^{(2)}(z) &= \left(\mathbf{N}^{(2)}\right)^{-1}\bar{\mathbf{N}}^{(1)}\bar{\mathbf{f}}'^{(1)}(z), \ x_2 < 0. \end{aligned} \tag{19}$$

Next consider the expressions for the derivative of the mechanical displacement jump and the electrical displacement jump

$$\langle \mathbf{v}(x_1) \rangle = \mathbf{v}^{(1)}(x_1 + i0) - \mathbf{v}^{(2)}(x_1 - i0)$$

over the bimaterial interface, which, in view of (14) and (19), takes the form

$$\langle \mathbf{v}(x_1) \rangle = \mathbf{D}\mathbf{f}'^{(1)}(x_1 + i0) + \bar{\mathbf{D}}\bar{\mathbf{f}}'^{(1)}(x_1 - i0),$$

where $\mathbf{D} = \mathbf{M}^{(1)} - \bar{\mathbf{M}}^{(2)} \left(\bar{\mathbf{N}}^{(2)}\right)^{-1} \mathbf{N}^{(1)}$. Here and afterward the brackets $\langle \ldots \rangle$ denote the jump of the corresponding function over the bimaterial interface.

From the condition (13), we have $\langle \mathbf{v}(x_1) \rangle = 0$ for $x_1 \in L$ or

$$\mathbf{D}\mathbf{f}'^{(1)}(x_1 + i0) = -\bar{\mathbf{D}}\bar{\mathbf{f}}'^{(1)}(x_1 - i0), \quad x_1 \in L.$$

We can introduce the vector-function $\mathbf{w}(z) = [w_1(z), w_2(z)]^{\mathrm{T}}$ by the formula

$$\mathbf{w}(z) = \begin{cases} \mathbf{D}\mathbf{f}'^{(1)}(z), & x_2 > 0, \\ -\bar{\mathbf{D}}\bar{\mathbf{f}}'^{(1)}(z), & x_2 < 0, \end{cases}$$

which is analytic in the whole plane cut along $(-\infty, \infty)\backslash L$ and tends to a constant as $|z| \to \infty$. Then the field variables at the bimaterial interface can be expressed via the boundary values of the function $\mathbf{w}(z)$ in such a way that

$$\langle \mathbf{v}(x_1) \rangle = \mathbf{w}^+(x_1) - \mathbf{w}^-(x_1), \tag{20}$$

$$\mathbf{p}(x_1, 0) = \mathbf{G}\mathbf{w}^+(x_1) - \bar{\mathbf{G}}\mathbf{w}^-(x_1), \tag{21}$$

where $\mathbf{G} = \mathbf{N}^{(1)} (\mathbf{D})^{-1}$ and the superscripts '+' and '−' indicate the limit values at the interface takes from the upper and the lower half-planes, respectively.

In this paper, as defined before, we consider transversely isotropic piezoelectric materials poled in the x_3-direction. For this case, the matrix $\mathbf{G}$ has the form

$$\mathbf{G} = \begin{bmatrix} ig_{11} & g_{12} \\ g_{21} & ig_{22} \end{bmatrix},$$

where all g_{kl} $(k, l = 1, 2)$ are real. Furthermore, taking into account the form of the matrix $\mathbf{G}$, the relation (21) can be written in the expanded form

$$\begin{aligned} \sigma_{23}(x_1, 0) &= ig_{11}w_1^+(x_1) + g_{12}w_2^+(x_1) + ig_{11}w_1^-(x_1) - g_{12}w_2^-(x_1), \\ E_1(x_1, 0) &= g_{21}w_1^+(x_1) + ig_{22}w_2^+(x_1) - g_{21}w_1^-(x_1) + ig_{22}w_2^-(x_1). \end{aligned} \tag{22}$$

Introducing the new functions

$$F_k(z) = w_2(z) + is_k w_1(z), \tag{23}$$

having the same properties as $\mathbf{w}(z)$, and combining the first and second equations (22) one arrives at the representations

$$\sigma_{23}(x_1, 0) - im_k E_1(x_1, 0) = t_k \left[F_k^+(x_1) + \gamma_k F_k^-(x_1)\right], \tag{24}$$

where

$$s_k = \frac{g_{11} - m_k g_{21}}{t_k}, \quad \gamma_k = -\frac{g_{12} - m_k g_{22}}{t_k}, \quad t_k = g_{12} + m_k g_{22}, \quad m_{1,2} = \mp\sqrt{-\frac{g_{11}g_{12}}{g_{21}g_{22}}}, \quad k = 1, 2.$$

On the other hand, according to (23)

$$F_k^+(x_1) - F_k^-(x_1) = w_2^+(x_1) - w_2^-(x_1) + is_k \left[w_1^+(x_1) - w_1^-(x_1)\right],$$

then using (20), one gets

$$\langle D_2(x_1) \rangle + is_k \left\langle u_3'(x_1) \right\rangle = F_k^+(x_1) - F_k^-(x_1). \tag{25}$$

Numerical analysis shows that the constants s_k, γ_k, t_k, m_k are real, and besides $s_{1,2} = -m_{1,2}$, $\gamma_2 = 1/\gamma_1$ hold true.

The expressions (24) and (25) play an important role in the following analysis because by means of these expressions the problems of linear relationship for various mixed boundary conditions at the interface can be formulated and successfully solved.

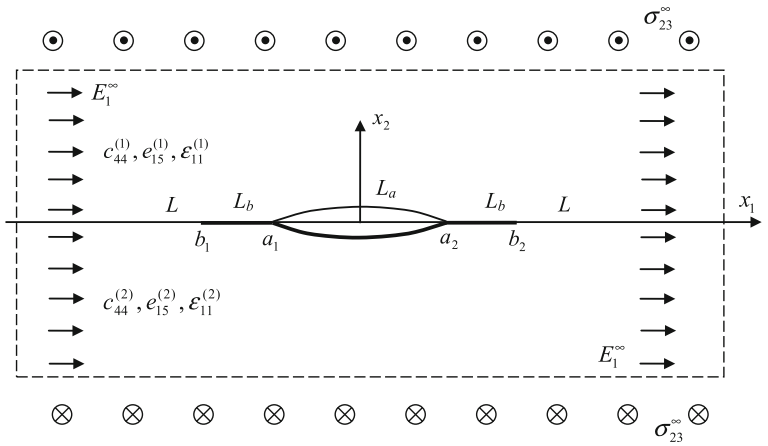

Fig. 1 The electrode–ceramic interface crack under the action of anti-plane mechanical and in-plane electric loadings

4 Problem formulation

We now focus on the fracture mechanical boundary value problem motivated in the introduction. Consider a finite internal electrode $b_1 \le x_1 \le b_2$ located at the interface $x_2 = 0$ between two dissimilar piezoelectric half-planes $x_2 > 0$ and $x_2 < 0$, as shown in Fig. 1. The upper and lower components of the bimaterial are piezoceramics with poling direction parallel to the x_3-axis and material properties $c_{44}^{(k)}$, $e_{15}^{(k)}$, and $\varepsilon_{11}^{(k)}$, where the mentioned values are the stiffness, piezoelectric, and dielectric constants, respectively ($k = 1$ stands for the upper half-plane and $k = 2$ for the lower one). Since the electrode is commonly more flexible than the piezoelectric material, its mechanical properties are neglected. Thus, the electrode is represented by its electrical properties, only. We suppose that outside the electrode the half-planes are mechanically and electrically bonded along the interface.

An anti-plane mechanical loading σ_{23}^{∞} and an in-plane electric loading E_1^{∞} are applied at infinity. This loading results in an anti-plane mechanical and in-plane electric state for which the relations (24) and (25) are valid.

It is assumed that this bimaterial compound contains a single electrode–ceramic interface crack $a_1 \le x_1 \le a_2$ ($b_1 \le a_1, a_2 \le b_2$), situated on one side of the electrode and that there is no traction and free charge on the crack surface. The crack is supposed to be electrically conducting.

The electrode–ceramic crack is denoted by $L_a = (a_1, a_2)$, and the electrode areas without crack by $L_b = (b_1, a_1) \cup (a_2, b_2)$, while the bonded parts of the interface are denoted by $L = (-\infty, b_1) \cup (b_2, \infty)$. Then the boundary conditions at the interface $x_2 = 0$ can be written as

$$\sigma_{23}^{+} = \sigma_{23}^{-} = 0, \quad E_1^{+} = E_1^{-} = 0, \quad x_1 \in L_a, \tag{26}$$

$$\langle \sigma_{23} \rangle = 0, \quad \langle \gamma_{13} \rangle = 0, \quad E_1^{+} = E_1^{-} = 0, \quad x_1 \in L_b, \tag{27}$$

$$\langle \gamma_{13} \rangle = 0, \quad \langle \sigma_{23} \rangle = 0, \quad \langle E_1 \rangle = 0, \quad \langle D_2 \rangle = 0, \quad x_1 \in L. \tag{28}$$

The field variables at the bimaterial interface can be represented by means of the expressions (24) and (25). Due to the method by which expressions are constructed, they automatically satisfy the boundary conditions $\langle \sigma_{23} \rangle = 0$ and $\langle E_1 \rangle = 0$ for the whole interface and, accordingly, satisfy the first and fourth interface conditions (28) for $x_1 \in L$. To satisfy the remaining boundary conditions (26) and (27), one gets with the use of (24) and (25) the equations

$$F_k^{+}(x_1) + \gamma_k F_k^{-}(x_1) = 0, \quad x_1 \in L_a, \tag{29}$$

$$\mathrm{Im}\left[F_k^{+}(x_1) + \gamma_k F_k^{-}(x_1)\right] = 0, \quad \mathrm{Im}\left[F_k^{+}(x_1) - F_k^{-}(x_1)\right] = 0, \quad x_1 \in L_b, \tag{30}$$

where the functions $F_k(z)$ are analytic in the whole plane cut along (b_1, b_2) of the interface and 'Im' denotes the imaginary part of an analytic function. The simultaneous satisfaction of both equalities (30) is possible only if the equation

$$\mathrm{Im} F_k^{\pm}(x_1) = 0, \quad x_1 \in L_b. \tag{31}$$

is valid.

Taking into account that for $x_1 \notin (-b_1, b_2)$ the relation $F_k^+(x_1) = F_k^-(x_1) = F_k(x_1)$ holds, the conditions at infinity for the functions $F_k(z)$ by using of Eq. (24) and the prescribed remote electromechanical loads can be written as

$$F_k(z)|_{z\to\infty} = \frac{\sigma_{23}^{\infty} - i m_k E_1^{\infty}}{t_k(1+\gamma_k)}. \tag{32}$$

5 Solution of the problem

For each $k = 1, 2$, the relations (29) and (31) are a homogeneous combined Dirichlet–Riemann problem of linear relationship. Considering that $\gamma_2 = 1/\gamma_1$, the solution of the problem in question for $k = 2$ can be obtained from the associated solution for $k = 1$. Therefore, our attention will now be focused only on the case $k = 1$. The general solution of (29) and (31) can be constructed by the method from Nakhmein and Nuller [17] and Govorukha et al. [5] and are presented as

$$F_1(z) = X(z)\,[P(z) + i\,Q(z)Y(z)]\,, \tag{33}$$

where

$$X(z) = \frac{e^{i\phi(z)}}{(z-d)\sqrt{(z-a_1)(z-a_2)}}, \quad Y(z) = \sqrt{\frac{(z-a_1)(z-a_2)}{(z-b_1)(z-b_2)}},$$

$$\phi(z) = -Z(z)\left(\varepsilon_1 \int_{a_1}^{a_2} \frac{\mathrm{d}t}{Z(t)(t-z)} + i\int_{b_1}^{a_1} \frac{h_1(t)\mathrm{d}t}{Z^+(t)(t-z)} + i\int_{a_2}^{b_2} \frac{h_2(t)\mathrm{d}t}{Z^+(t)(t-z)}\right), \quad \varepsilon_1 = \frac{\ln\gamma_1}{2\pi},$$

$$Z(z) = \sqrt{(z-b_1)(z-b_2)(z-a_1)(z-a_2)}, \quad h_1(x_1) = n^*, \quad h_2(x_1) = \begin{cases} 1, & x_1 \in (a_2, d), \\ 0, & x_1 \in (d, b_2), \end{cases}$$

n^* is an integer number, and $d \in (a_2, b_2)$ is an unknown pole of the function $X(z)$.

The integrals in the expression for the function $\phi(z)$ can be represented via elliptic integrals as [6]

$$\phi(z) = \frac{-2}{\sqrt{(b_2-a_1)(a_2-b_1)}}\left\{\varepsilon_1\sqrt{\frac{(z-a_2)(z-b_2)}{(z-a_1)(z-b_1)}}\phi_1(z) + n^*\sqrt{\frac{(z-a_1)(z-a_2)}{(z-b_1)(z-b_2)}}\phi_2(z) - \sqrt{\frac{(z-b_1)(z-b_2)}{(z-a_1)(z-a_2)}}\phi_3(z)\right\},$$

where

$$\mu = \arcsin\sqrt{\frac{(b_2-a_1)(d-a_2)}{(b_2-a_2)(d-a_1)}}, \tag{34}$$

and

$$\phi_1(z) = (a_1-b_1)\Pi(p_1, q) + (z-a_1)K(q), \quad p_1 = p_1^*\frac{z-b_1}{z-a_1}, \quad p_1^* = \frac{a_2-a_1}{a_2-b_1},$$

$$\phi_2(z) = (b_1-b_2)\Pi(p_2, r) + (z-b_1)K(r), \quad p_2 = p_2^*\frac{z-b_2}{z-b_1}, \quad p_2^* = \frac{b_1-a_1}{b_2-a_1},$$

$$\phi_3(z) = (a_2-a_1)\Pi(\mu, p_3, r) + (z-a_2)F(\mu, r), \quad p_3 = p_3^*\frac{z-a_1}{z-a_2}, \quad p_3^* = \frac{b_2-a_2}{b_2-a_1},$$

$$q = \sqrt{\frac{(a_2-a_1)(b_2-b_1)}{(b_2-a_1)(a_2-b_1)}}, \quad r = \sqrt{\frac{(b_2-a_2)(a_1-b_1)}{(b_2-a_1)(a_2-b_1)}}.$$

Here, $F(\mu, r)$ and $\Pi(\mu, p, r)$ are incomplete elliptic integrals of the first and third kind, while $K(r)$ and $\Pi(p, r)$ are complete elliptic integrals of the first and third kind.

The integer n^* and the pole d of the function $X(z)$ can be found from the finiteness conditions at infinity of the function $\phi(z)$, which has the form [15]

$$\varepsilon_1 \int_{a_1}^{a_2} \frac{\mathrm{d}t}{Z(t)} + i \int_{b_1}^{a_1} \frac{h_1(t)\mathrm{d}t}{Z^+(t)} + i \int_{a_2}^{b_2} \frac{h_2(t)\mathrm{d}t}{Z^+(t)} = 0. \tag{35}$$

Expressing the integrals in Eq. (35) via elliptic integrals [6], we can rewrite this equation as

$$F(\mu, r) = \varepsilon_1 K(q) + n^* K(r). \tag{36}$$

Since the elliptical integral $F(\mu, r)$ is positive and $F(\mu, r) < K(r)$, the last equation leads for n^* to the condition

$$-\varepsilon_1 \frac{K(q)}{K(r)} < n^* < 1 - \varepsilon_1 \frac{K(q)}{K(r)}.$$

Apparently, this condition uniquely determines the ratio n^*. Solving Eq. (36) with respect to μ and (34) with respect to d, one gets

$$d = \frac{a_1(b_2 - a_2)\mathrm{sn}^2(\omega, r) - a_2(b_2 - a_1)}{(b_2 - a_2)\mathrm{sn}^2(\omega, r) - b_2 + a_1}, \tag{37}$$

where $\mathrm{sn}(\omega, r)$ is the Jacobi elliptic function and $\omega = \varepsilon_1 K(q) + n^* K(r)$.

The functions $P(z)$ and $Q(z)$, appearing in the solution (33), have the form

$$P(z) = C_0 + C_1 z + C_2 z^2, \quad Q(z) = D_0 + D_1 z + D_2 z^2, \tag{38}$$

where the coefficients C_ς, $D_\varsigma (\varsigma = 0, 1, 2)$ are real constants. To determine the constants C_1, C_2, D_1, D_2 from the conditions at infinity (32) for the function $F_1(z)$, we use the expansion

$$Z(z)|_{z\to\infty} = z^2\left[1 + \xi_1/z + O(z^{-2})\right], \quad Y(z)|_{z\to\infty} = 1 + \eta_1/z + O(z^{-2}),$$
$$\phi(z)|_{z\to\infty} = \alpha_0 + \alpha_1/z + O(z^{-2}), \quad X(z)|_{z\to\infty} = z^{-2}e^{i\alpha_0}\left[1 + \rho_1/z + O(z^{-2})\right],$$

of the functions at infinity, where

$$\xi_1 = -\frac{1}{2}(a_1 + a_2 + b_1 + b_2), \quad \eta_1 = \frac{1}{2}(b_2 + b_1 - a_2 - a_1), \quad \alpha_0 = A_2, \quad \alpha_1 = \xi_1 A_2 + A_3,$$
$$\rho_1 = \nu_1 + i\alpha_1, \quad \nu_1 = \frac{a_1 + a_2}{2} + d,$$
$$A_\zeta = \varepsilon_1 \int_{a_1}^{a_2} \frac{t^{\zeta-1}\mathrm{d}t}{Z(t)} + i \int_{b_1}^{a_1} \frac{t^{\zeta-1}h_1(t)\mathrm{d}t}{Z^+(t)} + i \int_{a_2}^{b_2} \frac{t^{\zeta-1}h_2(t)\mathrm{d}t}{Z^+(t)}, \quad \zeta = 2, 3.$$

Substituting the above expressions into (33), we get

$$F_1(z)|_{z\to\infty} = e^{i\alpha_0}\left\{C_2 + iD_2 + \frac{1}{z}\left[C_1 + i(D_1 + \eta_1 D_2) + \rho_1(C_2 + iD_2)\right]\right\} + O(z^{-2}). \tag{39}$$

Comparing the right-hand sides of (32) and (39), we get the expressions

$$C_2 = \frac{\sigma_{23}^\infty \cos\alpha_0 - m_1 E_1^\infty \sin\alpha_0}{t_1(1 + \gamma_1)}, \quad D_2 = -\frac{\sigma_{23}^\infty \sin\alpha_0 + m_1 E_1^\infty \cos\alpha_0}{t_1(1 + \gamma_1)},$$

and

$$C_1 = \alpha_1 D_2 - \nu_1 C_2, \quad D_1 = -(\eta_1 + \nu_1) D_2 - \alpha_1 C_2.$$

for the coefficients. The remaining coefficients are determined from the condition of the absence of a pole at the point d, i.e.,

$$P(d) + iQ(d)Y^-(d) = 0, \quad P'(d) + iQ'(d)Y^-(d) + iQ(d)Y'^-(d) = 0,$$

which can be written as a system

$$C_0 + C_1 d + C_2 d^2 - \chi D_0 - \chi D_1 d - \chi D_2 d^2 = 0,$$
$$C_1 + 2C_2 d - \chi D_1 - 2\chi D_2 d - \chi^* D_0 - \chi^* D_1 d - \chi^* D_2 d^2 = 0$$

of linear algebraic equations where

$$\chi^* = \frac{1}{2\chi}\left[\frac{(2d - a_1 - a_2)(d - b_1)(b_2 - d) + (2d - b_1 - b_2)(d - a_1)(d - a_2)}{(d - b_1)^2(b_2 - d)^2}\right],$$
$$\chi = \sqrt{\frac{(d - a_1)(d - a_2)}{(d - b_1)(b_2 - d)}}.$$

Solving this system, we get

$$C_0 = -C_1\left(d - \frac{\chi}{\chi^*}\right) - C_2 d\left(d - \frac{2\chi}{\chi^*}\right) - \frac{\chi^2}{\chi^*}(D_1 + 2D_2 d),$$
$$D_0 = \frac{1}{\chi^*}(C_1 + 2C_2 d) - D_1\left(d + \frac{\chi}{\chi^*}\right) - D_2 d\left(d + \frac{2\chi}{\chi^*}\right).$$

Using the solution (33) together with the formulas (24) and (25), one gets

$$\sigma_{23}(x_1, 0) - im_1 E_1(x_1, 0) = \frac{t_1(1 + \gamma_1)}{x_1 - d}\left\{\frac{P(x_1)\cos\phi(x_1)}{\sqrt{(x_1 - a_1)(x_1 - a_2)}} - \frac{Q(x_1)\sin\phi(x_1)}{\sqrt{(x_1 - b_1)(x_1 - b_2)}}\right.$$
$$\left. + i\left[\frac{Q(x_1)\cos\phi(x_1)}{\sqrt{(x_1 - b_1)(x_1 - b_2)}} + \frac{P(x_1)\sin\phi(x_1)}{\sqrt{(x_1 - a_1)(x_1 - a_2)}}\right]\right\}, \quad x_1 > b_2, \tag{40}$$

$$\langle D_2(x_1)\rangle + is_1\left\langle u_3'(x_1)\right\rangle = \frac{1 + \gamma_1}{\sqrt{\gamma_1}(x_1 - d)}\left\{\frac{Q(x_1)\cos\phi^*(x_1)}{\sqrt{(x_1 - b_1)(b_2 - x_1)}} + \frac{P(x_1)\sin\phi^*(x_1)}{\sqrt{(x_1 - a_1)(a_2 - x_1)}}\right.$$
$$\left. + i\left[\frac{Q(x_1)\sin\phi^*(x_1)}{\sqrt{(x_1 - b_1)(b_2 - x_1)}} - \frac{P(x_1)\cos\phi^*(x_1)}{\sqrt{(x_1 - a_1)(a_2 - x_1)}}\right]\right\}, \quad x_1 \in (a_1, a_2), \tag{41}$$

$$\sigma_{23}(x_1, 0) = \frac{2t_1\sqrt{\gamma_1}\cos[\pi h_2(x_1)]}{x_1 - d}\left\{\frac{P(x_1)\cosh\left[\tilde\phi(x_1) - \pi\varepsilon_1\right]}{\sqrt{(x_1 - a_1)(x_1 - a_2)}}\right.$$
$$\left. + \frac{Q(x_1)\sinh\left[\tilde\phi(x_1) - \pi\varepsilon_1\right]}{\sqrt{(x_1 - b_1)(b_2 - x_1)}}\right\}, \quad x_1 \in (a_2, b_2), \tag{42}$$

$$\langle D_2(x_1)\rangle = \frac{2\cos[\pi h_2(x_1)]}{x_1 - d}\left\{\frac{P(x_1)\sinh\tilde\phi(x_1)}{\sqrt{(x_1 - a_1)(x_1 - a_2)}}\right.$$
$$\left. + \frac{Q(x_1)\cosh\tilde\phi(x_1)}{\sqrt{(x_1 - b_1)(b_2 - x_1)}}\right\}, \quad x_1 \in (a_2, b_2), \tag{43}$$

where

$$\phi^*(x_1) = -Z(x_1)\left[\varepsilon_1\int_{a_1}^{a_2}\frac{\mathrm{d}t}{Z(t)(t - x_1)} + i\int_{b_1}^{a_1}\frac{h_1(t)\mathrm{d}t}{Z^+(t)(t - x_1)} + i\int_{a_2}^{b_2}\frac{h_2(t)\mathrm{d}t}{Z^+(t)(t - x_1)}\right],$$
$$\tilde\phi(x_1) = -iZ^+(x_1)\left[\varepsilon_1\int_{a_1}^{a_2}\frac{\mathrm{d}t}{Z(t)(t - x_1)} + i\int_{b_1}^{a_1}\frac{h_1(t)\mathrm{d}t}{Z^+(t)(t - x_1)} + i\int_{a_2}^{b_2}\frac{h_2(t)\mathrm{d}t}{Z^+(t)(t - x_1)}\right].$$

Analysis of the formulas (40) and (42) shows that the stress $\sigma_{23}(x_1, 0)$ is singular for $x_1 \to a_2 + 0$ and $E_1(x_1, 0)$ is singular for $x_1 \to b_2 + 0$. In all mentioned cases, inverse square root singularities are found. Thus, the intensity factors for stress and electric field can be defined as

$$K_\sigma = \lim_{x_1 \to a_2 + 0} \sqrt{2\pi(x_1 - a_2)}\,\sigma_{23}(x_1, 0),$$
$$K_{\mathrm{E}} = \lim_{x_1 \to b_2 + 0} \sqrt{2\pi(x_1 - b_2)}\,E_1(x_1, 0). \tag{44}$$

Applying the formulas of Muskhelisvili [16] to Cauchy type integrals, which are expressed via the functions $\tilde{\phi}(x_1)$, $\phi^*(x_1)$ and $\phi(x_1)$ in the vicinity of singular points, one arrives at

$$\phi(b_2) = 0, \quad \phi^*(a_2) = 0, \quad \tilde{\phi}(a_2) = \pi\varepsilon_1.$$

Substituting these formulas into (40) and (42) and considering the obtained expressions in the vicinity of the points a_2 and b_2, we get

$$K_\sigma = \sqrt{\frac{8\pi\gamma_1}{a_2 - a_1}}\,\frac{t_1 P(a_2)}{d - a_2}, \quad K_{\mathrm{E}} = \sqrt{\frac{2\pi}{b_2 - b_1}}\,\frac{t_1(1 + \gamma_1)Q(b_2)}{m_1(d - b_2)}. \tag{45}$$

To confirm the validity of the obtained solution, let us suppose that the electrode areas without crack are absent and only the electrode–ceramic interface crack is situated along $b_1 \le x_1 \le b_2$. In this case, the homogeneous Hilbert problem

$$F_1^+(x_1) + \gamma_1 F_1^-(x_1) = 0 \quad \text{for} \quad b_1 \le x_1 \le b_2 \tag{46}$$

follows from (24), (26) and the conditions at infinity (32) are valid.

This problem is relatively simple and its solution can be easily found referring to Muskhelisvili [15] in the form

$$F_1(z) = \frac{\sigma_{23}^\infty - im_1 E_1^\infty}{t_1(1 + \gamma_1)}(z - b_1)^{-1/2 + i\varepsilon_1}(z - b_2)^{-1/2 - i\varepsilon_1}\left[z - i\varepsilon_1(b_2 - b_1) - \frac{b_1 + b_2}{2}\right]. \tag{47}$$

Substituting (47) into (24), we get the expressions

$$\sigma_{23}(x_1, 0) - im_1 E_1(x_1, 0) = \frac{\sigma_{23}^\infty - im_1 E_1^\infty}{\sqrt{(x_1 - b_1)(x_1 - b_2)}}\left(x_1 - i\varepsilon_1(b_2 - b_1) - \frac{b_1 + b_2}{2}\right)\left[\frac{x_1 - b_1}{x_1 - b_2}\right]^{i\varepsilon_1} \tag{48}$$

for the stress and electric field at the bonded part $x_1 > b_2$ of the bimaterial interface.

Considering the formula (40) for $a_1 \to b_1$ and $a_2 \to b_2$, we arrive exactly at Eq. (48). This fact confirms the correctness of the solution (33) and, moreover, it shows that the presence of the intact electrode areas $(b_1, a_1) \cup (a_2, b_2)$ transforms the oscillating singularity at the tips of an interface crack into two square root singularities at the points a_k and b_k $(k = 1, 2)$.

6 Numerical results and analysis

The numerical analysis has been performed for a bimaterial composed of commercially available piezoelectric ceramics PZT-4 (the upper material) and PZT-5H (the lower one). The material properties of these materials are taken from Park and Sun [22] and Pak [21], respectively, and $\sigma_{23}^\infty = 1$ MPa, $a_2 = 10$ mm are chosen for all calculations presented here. The analytical solution is obtained for any positions of the points a_1 and a_2. However, for the sake of clarity of the numerical illustrations it is assumed in this section that the centers of the electrode and the crack coincide with each other. Numerical results are presented for different ratios $\omega = (b_2 - b_1)/(a_2 - a_1)$. The main attention of the following numerical analysis will be devoted to the influence of the external electrical loading on the stress and electric field intensity factors as well as the spatial variations of the field variables at the bimaterial interface.

At the beginning, the variations of the crack faces' sliding displacement, i.e., the jump $\langle u_3(x_1)\rangle$ along the crack region (a_1, a_2), are displayed in Figs. 2a, b. Here and afterward the lines 1, 2 and 3 correspond to $E_1^\infty = 0$,

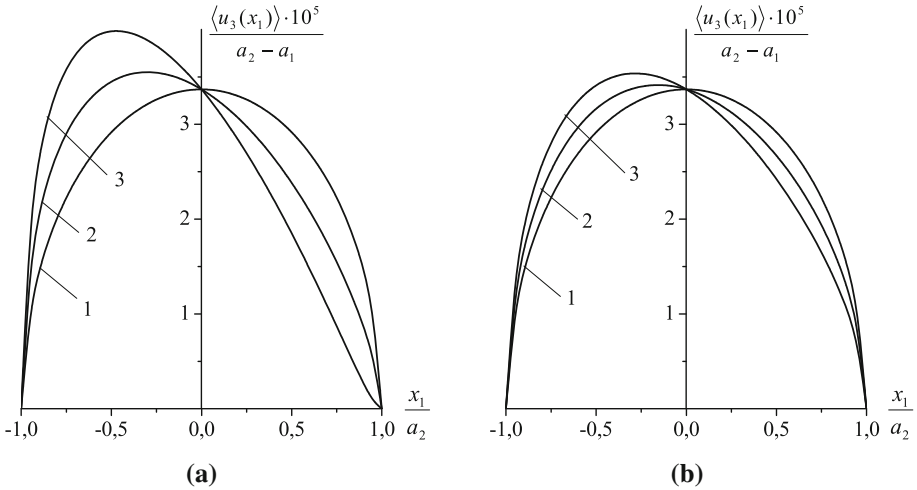

Fig. 2 The variation of the normalized crack faces sliding displacement jump along the crack region for $\omega = 1.1$ (**a**) and $\omega = 2.0$ (**b**)

Table 1 The variations of stress and electric field intensity factors for different intensities of the external electric field

E_1^∞ [V/m]	K_σ [Pa$\sqrt{\text{m}}$]		K_E [V/$\sqrt{\text{m}}$]	
	$\omega = 1.1$	$\omega = 2.0$	$\omega = 1.1$	$\omega = 2.0$
-8.8395×10^2	1.7726×10^5	1.7726×10^5	≈ 0	-1.7993×10^2
-5×10^2	1.7722×10^5	1.7725×10^5	71.365	-83.690
-1.6612×10^2	1.7719×10^5	1.7724×10^5	1.3342×10^2	≈ 0
0	1.7717×10^5	1.7723×10^5	1.6430×10^2	41.641
3×10^4	1.7439×10^5	1.7628×10^5	5.7404×10^3	7.5615×10^3
1.9076×10^6	≈ 0	1.1670×10^5	3.5473×10^5	4.7820×10^5
3×10^6	-1.0146×10^5	8.2031×10^4	5.5777×10^5	7.5203×10^5
5.5849×10^6	-3.4154×10^5	≈ 0	1.0382×10^6	1.3940×10^6

$E_1^\infty = 10^6$ V/m, and $E_1^\infty = 2 \times 10^6$ V/m, respectively. The obtained results confirm an essential influence of electrical loading upon the crack faces sliding displacement jump $\langle u_3(x_1)\rangle$. The asymmetry of the graphs (lines 2, 3) appears because of nonzero electric field. The maximum of the crack faces' sliding displacement jump increases as the electric field increases. Besides, under the same remote electrical loading, the amplitude of the crack faces' sliding displacement jump becomes higher as the ratio of ω decreases, i.e., the coefficient of the electrode and crack lengths decreases. But it should be noted that for a relatively small value of electrical loading, this dependence is rather small. It is also worth to mention that the curve 3 in Fig. 2a corresponds to the special combination of electromechanical loading caused the smooth crack closing (see line 6 of the Table 1 also). Therefore this curve has no vertical tangent and differs with respect to this feature from the other curves.

The distribution of the shear stress $\sigma_{23}(x_1, 0)$ along the bonded part $x_1 \in (a_2, b_2)$ of the electrode zone for different values of the external electrical loading are shown in Figs. 3a, b. It is seen that for a relatively small value of electrical loading, the values of the shear stress $\sigma_{23}(x_1, 0)$ are positive in most parts of the interval (a_2, b_2) and are negative only near the point b_2, i.e., at the edge of the electrode. A decrease in the external electric field leads to an increase in the zone of negative stress field. This behavior can be described by the stress intensity factor K_σ, defined by Eq. (45). The dashed lines in these figures correspond to the case of $K_\sigma = 0$. In this special case, the crack closes smoothly at the point a_2 and the stress $\sigma_{23}(x_1, 0)$ tends to zero at this point.

Figure 4a, b shows the shear stress $\sigma_{23}(x_1, 0)$ variations at the electrode continuation $x_1 > b_2$, i.e., in the bonded interface beyond the electrode. It is observed clearly from this figure that the value of $\sigma_{23}(x_1, 0)$ decreases with the increase in magnitude of the applied electrical loading. Thus, the analysis of Figs. 3 and 4 confirms the analytical conclusion that the shear stresses $\sigma_{23}(x_1, 0)$ tend to infinity at the electrode tip for $x_1 \to b_2 - 0$ and remain always limited for $x_1 \to b_2 + 0$. Therefore, this stress is not continuous at the electrode tip and tends to its nominal value for all x_1 much larger than the electrode length.

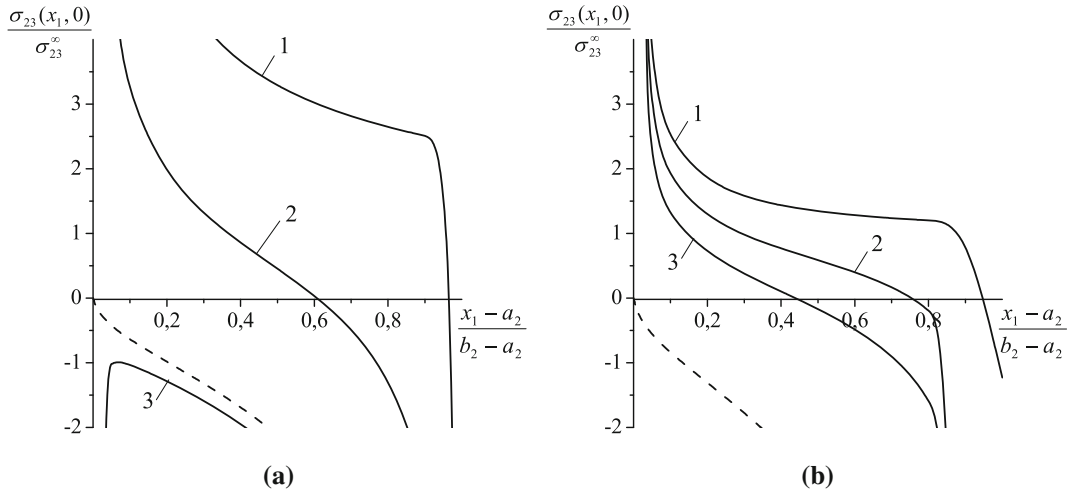

Fig. 3 Shear stress variation along the bonded electrode zone for $\omega = 1.1$ (**a**) and $\omega = 2.0$ (**b**)

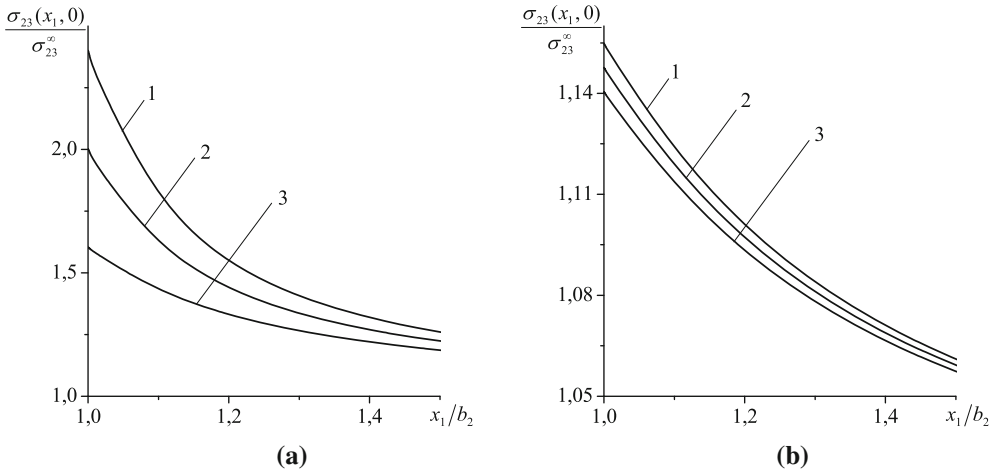

Fig. 4 Behavior of the shear stress at the electrode continuation for $\omega = 1.1$ (**a**) and $\omega = 2.0$ (**b**)

The variations of the electric field $E_1(x_1, 0)$ at the electrode continuation $x_1 > b_2$ are shown in Fig. 5. It is seen from this figure that $E_1(x_1, 0)$ is almost equal to 0 for $E_1^{\infty} = 0$, but it becomes rather large for a nonzero external electric field. In particular, $E_1(x_1, 0)$ is singular at the right neighborhood of the point b_2. Therefore, it grows very fast for x_1 tending to this point and it promptly decreases at a distance from it. However, the dependence of the electric field at the electrode continuation on the ratio of ω is negligibly small.

The variations of the stress intensity factor K_σ and of the electric field intensity factor K_{E} are shown in Table 1 for different values of ω and E_1^{∞}. It can be seen that the dependence of both K_σ and K_{E} on the electric field is rather essential. For each ω, the growing electrical loading E_1^{∞} leads to decrease in the stress intensity factor K_σ, eventually assuming vanishing values. This means that tuning of E_1^{∞} to an appropriate value decreases the danger of the crack development. On the other hand, the electric field intensity factor K_{E} is approximately proportional to the external electric field for large values of this field. For smaller absolute values of E_1^{∞}, the electric field intensity factor K_{E} is mostly defined by the external stress. Moreover, very small negative values of E_1^{∞} reduce the intensity factor K_{E} to zero.

7 Conclusions

The linear electroelastic problem for a piezoelectric bimaterial composite with an electrode–ceramic interface crack under the action of anti-plane mechanical and in-plane electric loadings has been analyzed. Due to a

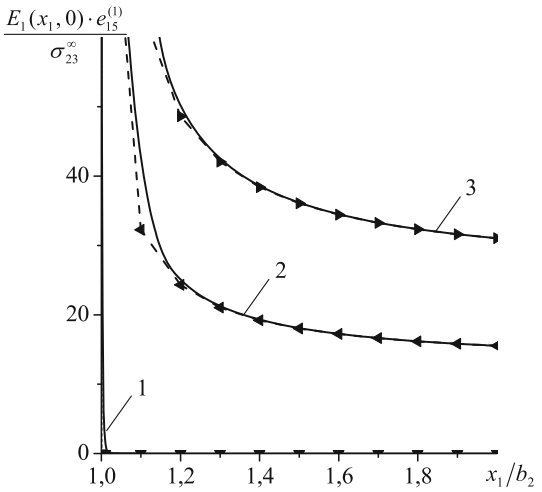

Fig. 5 Variation of the electric field at the electrode continuation for $\omega = 1.1$ (solid lines) and $\omega = 2.0$ (dashed lines with symbols)

special transformation of conventional representations (8), (9) of the field variables via analytical functions, the new representations (24), (25) convenient for the considered problem solution are found. On the basis of these representations, the problem is reduced to the combined Dirichlet–Riemann boundary value problem (29), (31) with the conditions (32) at infinity, and its exact analytical solution is derived. Due to the presence of an electrode at the crack continuation, the oscillating singularity at the tips of an interface crack transforms into two conventional square root singularities at the crack and the electrode tips for shear stress and electric field, respectively. Analytical expressions (40)–(43) for the field variables along the interface are presented in an explicit form. Furthermore, the stress and the electric field intensity factors (44) have been determined. The correctness of the obtained solution is confirmed by its comparison with the limiting case with the well-known solution for a single electrically conducting interface crack. The crack faces' sliding displacement, the electric field and the shear stress are calculated along the corresponding parts of the material interface and presented in a graphical form in Figs. 2, 3, 4 and 5 for different values of the external electric loading and different relations between the crack and electrode lengths. Furthermore, the stress and electric field intensity factors are presented in Table 1. The present investigation shows that an influence of the relation between the crack and electrode lengths on the field variables is almost absent for a relatively small value of electrical loading, but it becomes rather significant in the opposite case. The maximum of the crack face sliding displacement jump increases as the electric field increases. Besides, under the same remote electrical loading, the amplitude of the crack face sliding displacement jump becomes higher as the coefficient of the electrode and crack length decreases. Furthermore, the growth of the external electric field leads to a decrease in the stress intensity factor at the crack tip and to an increase in the electric field intensity factor at the electrode tip.

Acknowledgements Part of this work was executed during a stay of V. G. at Karlsruhe Institute of Technology (KIT). The authors gratefully acknowledge the support from KIT by funding the guest stay of V. G.

References

1. Deng, W., Meguid, S.A.: Analysis of conducting rigid inclusion at the interface of two dissimilar piezoelectric materials. J. Appl. Mech. **65**, 76–84 (1998)
2. dos Santos e Lucato, S.L., Lupascu, D.C., Kamlah, M.R., Rödel, J., Lynch, C.S.: Constraint-induced crack initiation at electrode edges in piezoelectric ceramics. Acta Mater. **49**, 2751–2759 (2001)
3. Furuta, A., Uchino, K.: Dynamic observation of crack propagation in piezoelectric multilayer actuators. J. Am. Ceram. Soc. **76**, 1615–1617 (1993)
4. Govorukha, V., Kamlah, M., Loboda, V., Lapusta, Y.: Interface cracks in piezoelectric materials. Smart Mater. Struct. **25**, 023001 (2016)
5. Govorukha, V., Kamlah, M., Loboda, V., Lapusta, Y.: An electrically permeable crack between two different piezoelectric materials. In: Wriggers, P., Eberhard, P. (eds.) Fracture mechanics of piezoelectric solids with interface cracks. Lecture Notes in Applied and Computational Mechanics, vol. 83, pp. 59–95. Springer (2017)
6. Gradshteyn, I.S., Ryzhik, I.M.: Tables of Integrals, Series and Products. Academic Press, New York (1965)

7. Häusler, C., Balke, H.: Full form of the near tip field for the interface crack between a piezoelectric material and a thin electrode. Mater. Sci. Forum **492–493**, 261–266 (2005)
8. Häusler, C., Gao, C.F., Balke, H.: Collinear and periodic electrode–ceramic interfacial cracks in piezoelectric bimaterials. J. Appl. Mech. **71**, 486–492 (2004)
9. Lang, S.: Harmonic functions. In: Axler, S., Ribet, K. (eds.) Complex Analysis. Graduate Texts in Mathematics, vol. 103, pp. 241–290. Springer, New York (1999)
10. Lapusta, Y., Onopriienko, O., Loboda, V.: An interface crack with partially electrically conductive crack faces under anti-plane mechanical and in-plane electric loadings. Mech. Res. Commun. **81**, 38–43 (2017)
11. Li, X.F., Duan, X.Y.: Electroelastic analysis of a piezoelectric layer with electrodes. Int. J. Fract. **111**, L73–L78 (2001)
12. Li, X.F.: Electroelastic field induced by thin interface electrodes between two bonded dissimilar piezoelectric ceramics. Sci. China Ser. G Phys. Mech. Astron. **49**, 526–539 (2006)
13. Li, Y.D., Zhang, N., Lee, K.Y.: Effect of a finite interface on the electrode in a non-homogeneous piezoelectric structure. Smart Mater. Struct. **18**, 125028 (2009)
14. Loboda, V., Mahnken, R.: An investigation of an electrode at the interface of a piezoelectric bimaterial space under remote electromechanical loading. Acta Mech. **221**, 327–339 (2011)
15. Muskhelishvili, N.I.: Some Basic Problems of Mathematical Theory of Elasticity. Noordhoff, Groningen (1953a)
16. Muskhelisvili, N.I.: Singular Integral Equations. Noordhoff, Groningen (1953b)
17. Nakhmein, E.L., Nuller, B.M.: The pressure of a system of stamps on an elastic half-plane under general conditions of contact adhesion and slip. J. Appl. Math. Mech. **52**, 223–230 (1988)
18. Narita, F., Yoshida, M., Shindo, Y.: Electroelastic effect induced by electrode embedded at the interface of two piezoelectric half-planes. Mech. Mater. **36**, 999–1006 (2004)
19. Onopriienko, O., Loboda, V., Sheveleva, A., Lapusta, Y.: Interaction of a conductive crack and of an electrode at a piezoelectric bimaterial interface. C. R. Mec. **346**, 449–459 (2018)
20. Pak, Y.E.: Crack extension force in a piezoelectric material. J. Appl. Mech. **57**, 647–653 (1990)
21. Pak, Y.E.: Linear electro-elastic fracture mechanics of piezoelectric materials. Int. J. Fract. **54**, 79–100 (1992)
22. Park, S.B., Sun, C.T.: Fracture criteria for piezoelectric ceramics. J. Am. Ceram. Soc. **78**, 1475–1480 (1995)
23. Parton, V.Z., Kudryavtsev, B.A.: Electromagnetoelasticity. Gordon and Breach, New York (1998)
24. Ru, C.Q.: Exact solution for finite electrode layers embedded at the interface of two piezoelectric half-planes. J. Mech. Phys. Solids **48**, 693–708 (2000a)
25. Ru, C.Q.: Electrode–ceramic interfacial cracks in piezoelectric multilayer materials. J. Appl. Mech. **67**, 255–261 (2000b)
26. Wang, B.L., Sun, Y.G., Han, J.C., Du, S.Y.: An interface electrode between two piezoelectric layers. Mech. Mater. **41**, 1–11 (2009)
27. Wang, X., Schiavone, P.: Debonded arc-shaped interface conducting rigid line inclusions in piezoelectric composites. C. R. Mec. **345**, 724–731 (2017)
28. Wang, X., Shen, Y.P.: Exact solution for mixed boundary value problems at anisotropic piezoelectric bimaterial interface and unification of various interface defects. Int. J. Solids Struct. **39**, 1591–1619 (2002)
29. Winzer, S.R., Shankar, N., Ritter, A.: Designing cofired multilayer electrostrictive actuators for reliability. J. Am. Ceram. Soc. **72**, 2246–2257 (1989)